LOS ALAMOS SCIENTIFIC LABORATORY
of the
University of California
LOS ALAMOS • NEW MEXICO

Neutron Flux Determination in Time-of-Flight Cross-Section Measurements Using Underground Nuclear Explosions

UNITED STATES
ATOMIC ENERGY COMMISSION
CONTRACT W-7405-ENG. 36

This report expresses the opinions of the author or authors and does not necessarily reflect the opinions or views of the Los Alamos Scientific Laboratory.

Printed in the United States of America. Available from
Clearinghouse for Federal Scientific and Technical Information
National Bureau of Standards, U. S. Department of Commerce
Springfield, Virginia 22151
Price: Printed Copy $3.00; Microfiche $0.65

Written: May 20, 1969
Distributed: February 5, 1970

LA-4095
UC-34, PHYSICS
TID-4500

LOS ALAMOS SCIENTIFIC LABORATORY
of the
University of California
LOS ALAMOS • NEW MEXICO

Neutron Flux Determination in Time-of-Flight Cross-Section Measurements Using Underground Nuclear Explosions

by

W. K. Brown
P. A. Seeger
M. G. Silbert

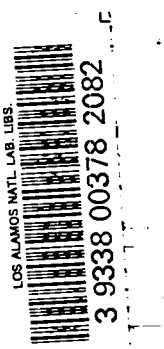

CONTENTS

GLOSSARY OF SYMBOLS

a	term in stopping cross-section formula, Eq. (20) (10^{-15} MeV-eV-cm^2/molecule).
A	atomic weight; collimator orifice area (cm^2).
A_0	standard collimator orifice area ($\equiv$ 3 cm^2).
b	term in stopping cross-section formula, Eq. (20) (ℓn 1/MeV).
C	center-of-mass system.
d	detector dead layer thickness (μm).
$D(t)$	particle detection rate (particles/sec).
e	energy-conversion efficiency of Moxon-Rae detectors: energy observed in detector per unit gamma-ray energy incident on the converter (dimensionless).
E	neutron energy (eV or MeV).
E_{av}	average energy.
E_c	charged particle energy.
$E_{dep}(E)$	energy deposited in detector as observable ionization.
$E(t)$	neutron energy, uniquely related to t, Eq. (1), for a particular experiment where ℓ is fixed.
$E_{c0}(E)$	energy of a charged particle entering an energy-degrading material.
$E_3(E)$	initial energy of a particle emitted from a nuclear reaction.
$I(E)$	neutron beam spectrum differential, $\equiv \frac{dI}{dE}$ (neutrons/eV, at E).
$I(t)$	total neutron beam current differential, $\equiv \frac{dI}{dt}$ (neutrons/sec, at t).
$I'(t)$	total beam current differential obtained in a particular experiment normalized to A_0 and Y_0 for comparison with those of other experiments.
kt	unit of energy release in a nuclear explosion (kilotons of high explosive equivalent).
ℓ	neutron flight path (m).
ℓ_0	standard neutron flight path, $\ell_0 \equiv$ 200 m.
ℓ_{ref}	neutron flight path to a designated target used as a reference on a particular experiment.
L	laboratory system.
m	mass.
M_3	mass of a particle emitted from a nuclear reaction (atomic weight).
$n(E)$	neutron beam spectrum differential, $\equiv \frac{dn}{dE}$ (neutrons/cm^2 eV, at E).
$n(t)$	neutron beam current differential, $\equiv \frac{dn}{dt}$ (neutrons/cm^2 sec, at t).
N	molecular density (molecules/cm^3).
N_d	areal density of detector atoms (atoms/barn).
N_s	areal density (atoms/cm^2 or 10^{15} atoms/cm^2).
Q	nuclear reaction energy (MeV).
R_{amp}	amplifier input impedance (ohms).
$R(t)$	nuclear reaction rate (reactions/sec).
S	total neutron yield from explosion source (neutrons).
$S(E)$	differential neutron spectrum of explosion source, $\equiv \frac{dS}{dE}$ (neutrons/eV, at E).
t	neutron flight time (μsec).
T	ratio of transmitted to incident neutron beam current (dimensionless).
v	velocity (m/μsec).
$V(t)$	voltage signal at amplifier input as a function of t (volts).
x	path length in stopping material (cm).
Y	yield of nuclear explosive in kt.
Y_0	standard yield for comparison of neutron currents and spectra; $Y_0 \equiv (\ell/200)^3$.
Z	atomic number.
α	ratio of efficiencies of incident and transmitted beam current detectors in transmission measurements (dimensionless).
ϵ	atomic stopping cross section (10^{-15} eV-cm^2/molecule).
θ	detector angle with respect to neutron beam direction.
ρ_s	Total areal density of deposited target material (e.g., oxide) normal to target surface (mg/cm^2).
σ_0	neutron cross section at 2200 m/sec (cm^2, barn).
$\sigma(E)$	neutron cross section at energy E.
$\frac{d\sigma}{d\Omega}$	differential cross section (cm^2/sr or barns/sr).
φ	azimuthal angle.
$\omega(\theta_L,\theta_C)$	C-to-L conversion factor (dimensionless).
Ω	target-detector solid angle (steradian).

NEUTRON FLUX DETERMINATION IN TIME-OF-FLIGHT CROSS-SECTION MEASUREMENTS USING UNDERGROUND NUCLEAR EXPLOSIONS

by

W. K. Brown, P. A. Seeger, and M. G. Silbert

ABSTRACT

Time-of-flight measurements of neutron cross sections involve determination of the neutron-beam flux by use of various "flux monitors." The unique features of the Los Alamos Scientific Laboratory explosion-source measurements have necessitated development of special instruments and methods for the flux determination for each type of reaction studied. General measurement techniques and neutron-beam flux characteristics are reviewed. Properties of flux monitors for fission, capture, and scattering, and for low neutron energies are discussed, as well as total cross-section measurement by transmission. Computer programs for data reduction are outlined, and the scheme for handling the propagation of errors is presented.

1. INTRODUCTION

The Los Alamos Scientific Laboratory is engaged in the time-of-flight measurement of neutron cross sections using underground nuclear-explosion sources.[1] The source generates an extremely intense neutron pulse. A well-collimated beam passes through targets at the end of a known flight path (see Fig. 1). Signals from detectors placed close to the targets are directly proportional to the cross section of the reaction and to the neutron flux, which is essentially the same through all targets. Therefore, a convenient intermediate step in determining unknown cross sections is the determination of the time-dependent neutron flux using one or more targets of known cross section. It is also necessary to predict the flux with reasonable accuracy before the experiment in order to preset recording sensitivities to prevent loss or compromise in quality of data because of limitations in the dynamic range of the recording system.[2]

Flux-measurement techniques in this type of experiment differ in one major aspect from conventional laboratory techniques. Because only a single pulse is available, enough events must be detected in each resolved time interval to give adequate statistical accuracy. The high reaction rates preclude use of conventional counting circuitry, and the data are in the form of current signals whose levels depend in part on the energy deposited per particle and on the cross section of the flux monitor. Because high signal levels are necessary to limit the effect of amplifier noise and baseline uncertainty, the Q-value of the reaction is as important as the cross section. This fact weighs against the use of hydrogen elastic scattering, for example, as a flux monitor, and supports the use of fissionable targets. However, at the lower end of the scale of available neutron energy (tens of eV), the large fluctuations in fission cross sections make preferable the use of (n,p) and (n,α) reactions on light nuclei, as commonly used in laboratory measurements. It is advantageous to use a flux monitoring reaction similar to the unknown to be measured, in order to reduce background and efficiency uncertainties when taking signal ratios.

Besides precision recording of the signal currents, absolute flux determination or cross-section ratio determination requires accurate measurement

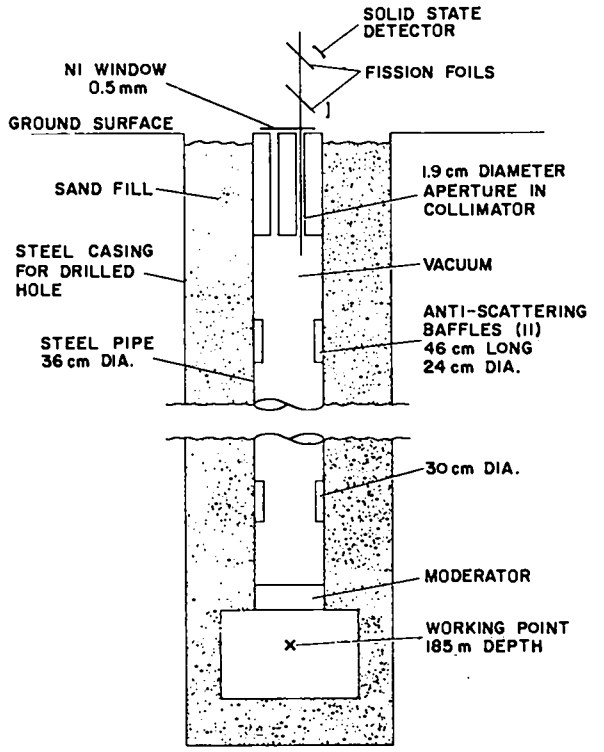

Fig. 1. A diagram of the experimental apparatus for neutron time-of-flight cross-section measurements. The nuclear explosion source is at the "working point" which was 185 m underground for this, the Petrel, event.

of monitor target thicknesses and target-detector solid angles. Methods for measuring these quantities and for calculating the energy losses of the various charged particles are described below.

Processing[3] of the background and flux monitor signals after data collection begins with the digitization of analog signal traces recorded on photographic film. The digitized data are converted to signal across the amplifier input in mV vs time of flight in μsec by the use of amplitude and time calibrations recorded on the film along with the data. The background is then subtracted from each signal, and each is divided by its cross section and multiplied by appropriate geometrical and kinematic factors to obtain the flux. Finally, the fluxes determined from various signals are combined by weighted averaging. Random and systematic uncertainties are propagated through each step.

2. DISCUSSION OF METHOD

a. Time-of-Flight Principles

For neutrons, the relation between energy, flight path, and time of flight is given by

$$E = \frac{1}{2} mV^2 = \frac{\ell^2}{t^2} (5226.95 \text{ eV } \mu\text{sec}^2 \text{ m}^{-2}). \qquad (1)$$

Typical flight paths used in explosion-source measurements are 200- to 300-m long. By placing a moderator in the line of sight above (or beside) the explosion source, as indicated in Fig. 1, an energy spectrum between 10 eV and several MeV is obtained. Fission neutrons begin to arrive at the targets after 10 to 20 μsec, and the last neutrons in about 5 msec; this defines the required recording time span.

The time resolution in the neutron beam depends on the 0.1-μsec burst time, the physical size of the source, and (at lower energies) the source time of the moderator. The rather complicated result of these combined effects has been discussed elsewhere.[1,4] All other system components are designed to match the shortest time, 0.1 μsec, associated with the source.

To achieve a nominal statistical accuracy of 3% in the analog signal, it is necessary to plan the experiment so as to obtain 1000 detected events per resolved time interval. The first step in planning for such a level is to obtain advance knowledge of the approximate neutron spectrum. Calculations both from theory and from previous experimental results are discussed in Section 3.

b. Current-Signal Principles

The reaction rate, R(t), is the product of the total neutron beam current, I(t), and the reaction probability, which for thin targets is the average target thickness parallel to the beam, N_s (atoms/cm^2), times the nuclear cross section, σ(E(t)):

$$R(t) = I(t) N_s \sigma(E). \qquad (2)$$

The quantities denoting beam current, I, and spectrum, n, are related by

$$I(t)dt = A\, n(t)dt = A\, n(E)dE = I(E)dE, \qquad (3)$$

where A is the collimator orifice area. Above the orifice, I(E) is independent of the distance from the source; I(t) for neutrons of fixed energy is inversely proportional to the flight path. The area of reacting material on the target foils is normally made larger than the beam, so that only the target

density and the total beam current enter into the calculation of the reaction rate.

Detectors appropriate to the type of measurement being performed are placed just outside the neutron beam, and view the reaction area on the target foil. For particles that always cause a pulse when they strike the detector (e.g., charged particles in a solid-state detector), the detected particle rate is given by

$$D(t) = I(t)N_s \frac{d\sigma}{d\Omega_L}(E,\theta_L)\Omega_L, \quad (4)$$

where the differential cross section in the laboratory, L, coordinate system is evaluated at the angle θ_L of the detector, and Ω_L is the laboratory solid angle of the detector, evaluated by integration over both the reaction area and the sensitive area of the detector.[1] If the angular distribution varies markedly over the angular spread involved, the integral should be so weighted. The relative solid angles of all detectors are measured in situ before each experiment by inserting an alpha source shaped like the reaction area into each target foil position.

If θ_C is the center-of-mass angle corresponding to θ_L, Eq. (4) is equally valid in the center-of-mass system if the detector solid angle is corrected by

$$\omega(\theta_L,\theta_C) \equiv \frac{d\Omega_C}{d\Omega_L} = \frac{\sin\theta_C d\theta_C d\varphi}{\sin\theta_L d\theta_L d\varphi}$$

$$= \frac{\sin^2\theta_C}{\sin^2\theta_L}\cos(\theta_C - \theta_L), \quad (5)$$

where the last equality is a result of nuclear kinematics. Then

$$D(t) = I(t)N_s \frac{d\sigma}{d\Omega_C}(E,\theta_C)\Omega_L\omega(\theta_L,\theta_C). \quad (6)$$

For s-wave neutrons, the angular distribution in the center-of-mass system is isotropic, $d\sigma/d\Omega_C = \sigma/4\pi$. Combining this with Eqs. (2) and (6),

$$D_{s\text{-wave}}(t) = R(t)(\Omega_L/4\pi)\,\omega(\theta_L,\theta_C) \approx R(t)\frac{\Omega_L}{4\pi}, \quad (7)$$

where the approximation is for low neutron energies for which $\omega = 1$.

Finally, the voltage signal, V(t), is the product of the detector current and the amplifier input impedance, R_{amp}:

$$V(t) = \frac{q\,D(t)E_{dep}(E)}{W}R_{amp}$$

$$= D(t)E_{dep}(E)R_{amp}(4.43 \times 10^{-8}\ \mu C\ MeV^{-1}), \quad (8)$$

where $E_{dep}(E)$ is the energy deposited per particle and W = 3.62 eV[5] is the energy required to create an ion pair in the Si detector. Electronic charge $q = 1.6 \times 10^{-13}$ μC. The calculation of $E_{dep}(E)$ for different types of measurements will be considered in the following sections. Note that uncertainties in W or q cancel because all measurements are ratios of two signals.

A second criterion can now be applied to the signal, in addition to the requirement on D(t) for adequate statistical accuracy. The signal must be large enough that it is not significantly affected by stray currents induced after the detonation of the nuclear explosive. The amplifiers used have lin-log gain characteristics capable of accepting input signals varying over several decades of dynamic range. Experience has shown that we cannot achieve 3% accuracy for V(t) of less than 0.5 mV using "high-gain" amplifiers or for V(t) of less than 3 mV using "low-gain" amplifiers.[1]

3. NEUTRON-FLUX CHARACTERISTICS

a. Prediction from Theory

The total number of neutrons produced by a nuclear explosive can be estimated from its energy yield. Given the yield in kilotons, using the standard conversion factors (1 lb TNT = 2×10^{13} ergs and 1 ^{235}U fission = 200 MeV), and estimating that of the 2.5 neutrons produced per fission 1.1 are consumed in producing the next generation, we calculate that a yield of about 3 kt is required to produce 1 mole of neutrons, more or less, depending on the neutron absorption in materials surrounding the nuclear explosive.

The shape of the neutron spectrum can be estimated from the fission spectrum.[6] The source is surrounded by hot (~ 1 keV) hydrogenous material (high explosive) at the time of neutron emission.[4] If a moderator is used, the typical 1/E slowing-down spectrum and Maxwellian "thermal" distribution of the heated, shocked, and moving moderator material are also present. If there is no moderator (as in the 1964 Parrot event), the typical source spectrum, S(E), can be normalized to the total neutron yield, S, by

$$S = \int_0^\infty S(E)\, dE, \tag{9}$$

and the observed neutron current will be S(E) reduced in magnitude by the fractional solid angle subtended by the collimator orifice.

When a moderator (usually polyethylene, somewhat protected from gamma heating by a lead sheath) is placed between the source and the collimator, some of the fast neutrons are removed from the beam. Of those removed, some leak from the moderator while slowing down, some are thermalized, and some are captured. Because neutrons leak from the moderator in all directions, the leakage must be considered a second source, typically separated from the source of fission neutrons by 1/2 m. The moderator is heated initially by gammas and neutrons to about 10 eV, and is compressed, heated, and accelerated by a strong shock after about 4 μsec. At that time, most of the neutrons are boiled and squeezed out of the moderator in a sharp-rising pulse having an exponential tail with a 1- to 2-μsec time constant. The bulk motion of the moderator up the flight path sets a lower limit on the neutron velocity.

The nuclear explosive may be placed out of the line of sight to prevent the high-intensity gamma flash from reaching the targets. This geometry eliminates the possibility of seeing fast neutrons direct from the device; the moderator is the sole source of neutrons. In this case, it is even more difficult to predict the spectrum; a Monte Carlo-type calculation is required.

b. Shot-to-Shot Comparison

Because of the difficulties and uncertainties in calculating the beam spectrum, further confidence can be obtained by intercomparison of the spectra obtained in previous experiments. This process is facilitated by adopting a standard reference flight path, collimator orifice, and explosive yield.

The beam current, I(E), is related to the source spectrum by the solid-angle ratio of the collimator orifice:

$$I(E) = \frac{A}{4\pi \ell^2} S(E). \tag{10}$$

A major factor affecting the current magnitude is the fact that if a higher yield device is used, it must be buried deeper to prevent escape of radioactive debris. In such experiments, in which a relatively large vacuum pipe extends to the surface, the depth-to-yield relationship has been approximately

$$\ell = 180\, Y_0^{1/3}, \tag{11}$$

where Y_0 approximates the actual yield and can be considered a nominal yield in kilotons defined by this relation. Because the number of neutrons produced is proportional to the yield, and yield is related to flight path by Eq. (11), the beam current per unit time is

$$I(t) = I(E)\left|\frac{dE}{dt}\right| \propto \frac{A}{\ell^2}\, \ell^3\, \frac{E^{3/2}}{\ell} = AE^{3/2}. \tag{12}$$

Thus, the beam current, I(t)/A, plotted vs E should be directly comparable from shot to shot, and the signal level at any energy from the same target should also be the same, unless the type or arrangement of the nuclear explosive or moderator is changed. Including variations of the orifice area and deviations of the actual yield from $Y_0(\ell)$, the properly normalized quantity for comparison is

$$I'(t) = I(t)\left(\frac{A}{A_0}\frac{Y}{Y_0}\right)^{-1}, \tag{13}$$

where the collimator orifice has been normalized to $A_0 \equiv 3\ cm^2$ to retain the units of current. Table I lists the pertinent quantities (where available) for four events. The beam currents for these events, normalized to aid in prediction of neutron currents in future events, are plotted in Fig. 2.

TABLE I

SHOT CHARACTERISTICS FOR FLUX COMPARISON

Event	Date	ℓ(m)	A(cm^2)	Y(kT)	Y_0(kT)	$\left(\frac{A}{A_0}\frac{Y}{Y_0}\right)$	$\left(\frac{\ell}{\ell_0}\frac{Y}{Y_0}\right)$
Parrot	Dec. 1964	181.3	1.04	1.2	1.02	0.41	1.07
Petrel	June 1965	181.3	2.85	1.2	1.02	1.12	1.07
Persimmon	Feb. 1967	300.6	2.97	N. A.	4.66		
Pommard	March 1968	214.6	2.97	1.3	1.69	0.76	0.83

$A_0 = 3\ cm^2$, $\ell_0 = 200$ m. $Y_0 = \left(\frac{\ell}{180}\right)^3$.

To predict a current for a future experiment, one uses

$$I(t)_{predicted} = \left(\frac{A}{A_0}\frac{Y}{Y_0}\right) I'(t)_{past}. \tag{14}$$

Such a prediction must be used with caution, particularly if any fundamental change is made in the nuclear explosive or moderator or in their arrange-

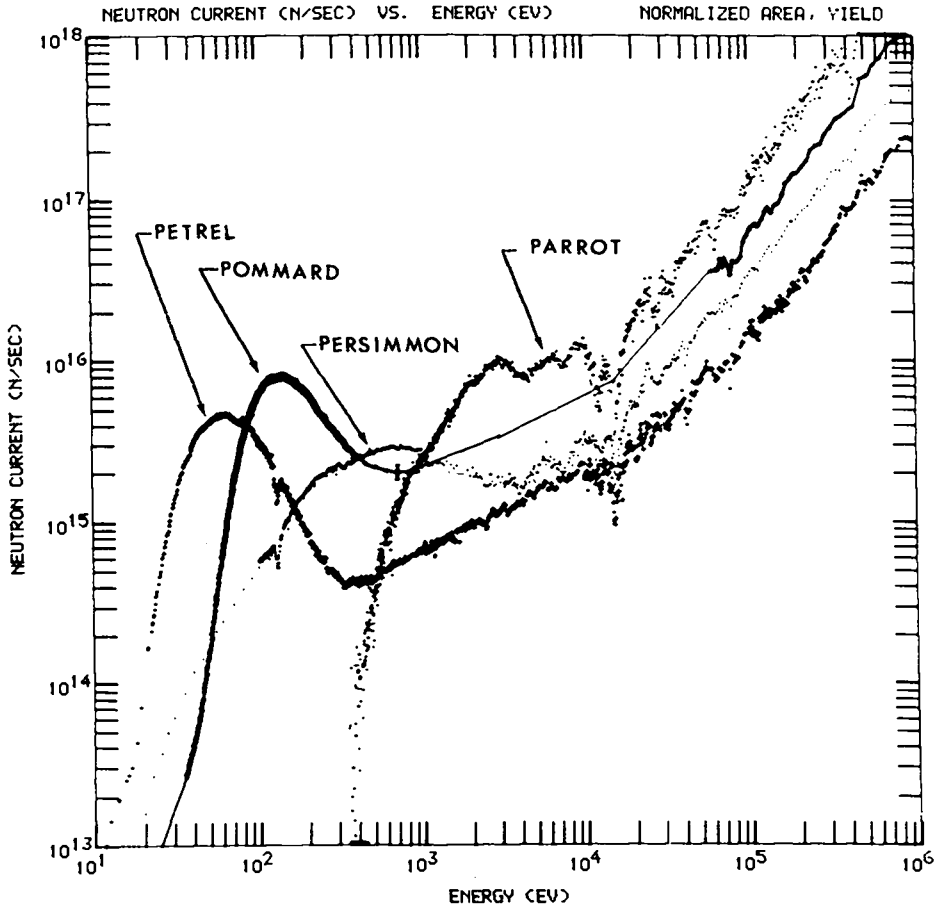

Fig. 2. Total neutron current vs neutron energy.

ment and location with respect to the line of sight. If changes are not too drastic, and nothing unforeseen occurs, it should be possible to predict the beam current in a future event to within a factor of two or three over at least part of the energy range.

Plots of neutron current such as those in Fig. 2, although in the most useful form for prediction of reaction rates, do not offer a basis of comparison to those familiar with various accelerator neutron sources, (α,n) sources, or nuclear reactors. Moreover, the $I'(t)$ vs E plot is not esthetically pleasing because it involves a time-varying quantity plotted vs energy, and is certainly not directly integrable in any sense. For these reasons, Fig. 3 has been included to display plots of $E \cdot n(E)$ vs E. This figure shows the actual (unnormalized) spectra obtained in the various events. Inspection of the foregoing equations reveals that if one wished to normalize the energy-dependent flux in the sense given above, the proper plots for comparison would be

$$n(E)\left(\frac{\ell}{\ell_0}\frac{Y}{Y_0}\right)^{-1} \quad \text{or} \quad E \cdot n(E)\left(\frac{\ell}{\ell_0}\frac{Y}{Y_0}\right)^{-1} \text{ vs } E,$$

where ℓ_0, an arbitrarily chosen flight path of typical 200-m length, has been introduced for convenience in retaining the spectrum units. The normalization factor has been included in Table I.

Graphical display of flux in the $E\,n(E)$ or $E\,I(E)$ form is convenient for several reasons. If the cross section of the target nucleus (or the target/detector combination) exhibits 1/v behavior and the cross section σ_0 at v = 2200 m/sec is known, then

$$\sigma(E) = \sigma_0 \frac{2200}{v} = 0.0022\,\sigma_0 \frac{t}{\ell}. \tag{15}$$

Because

$$I(t) = I(E)\left|\frac{dE}{dt}\right| = 2\frac{E}{t}\,I(E), \tag{16}$$

the reaction rate from Eq. (2) is proportional to

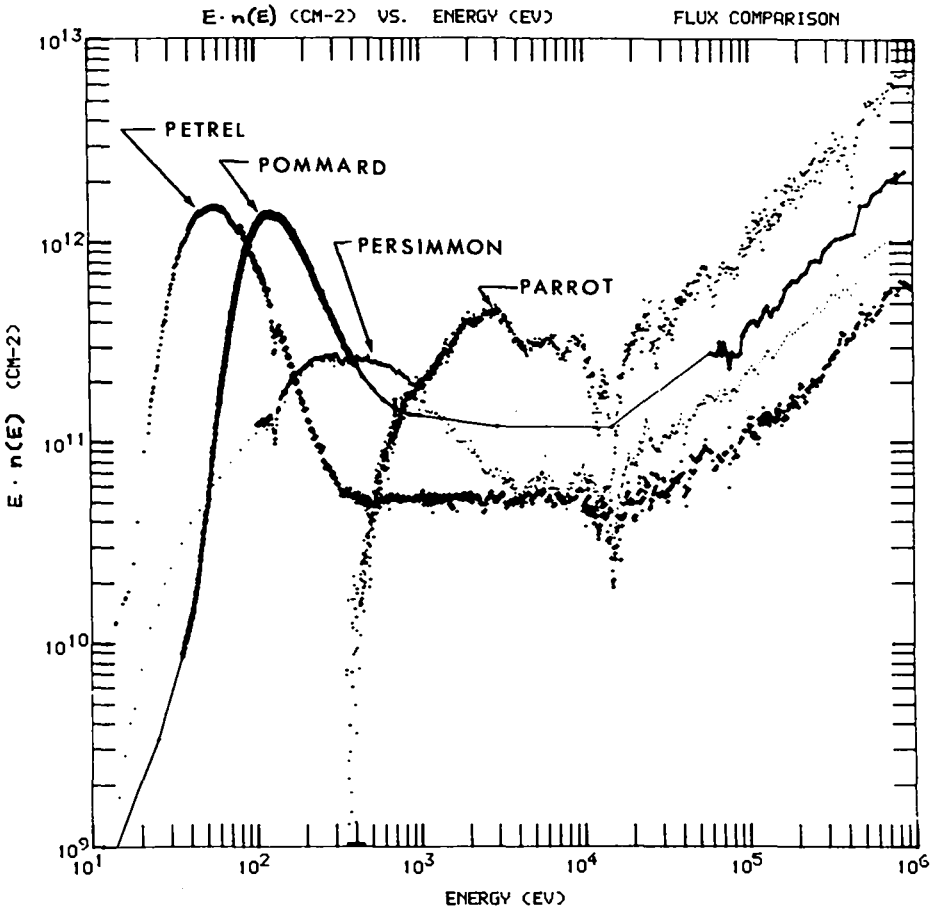

Fig. 3. Comparison of neutron spectra from the Parrot, Petrel, Persimmon, and Pommard events. The ordinate is in units of neutrons/eV-cm^2 multiplied by the neutron energy in eV.

E I(E):

$$R(t) = 2\ E\ I(E)\ N_s \frac{0.0022\ \sigma_0}{\ell}. \qquad (17)$$

Further, if $I(E) \propto 1/E$, as in the moderator slowing-down spectrum, then E I(E) and, hence, R(t) are constant in this energy range--an optimum result as is discussed below. Thus, a 1/E spectrum appears as a horizontal line on this type of plot and gives rise to a constant signal in the 1/v case. The E I(E) form obviates the need for plotting over many decades for this type of spectrum (as in the I(E) case) and therefore displays greater detail. This type of plot has become standard among health physicists and reactor physicists, who will recognize the ordinate units as being neutrons per unit "lethargy," i.e., per natural logarithmic energy decrement. Note that when flux is plotted vs log E, the unit energy changes in length along the abscissa, whereas the logarithmic energy decrement does not.

c. Optimum Spectrum Shape

For the purposes of this method of neutron cross-section measurement, an optimum spectrum (besides being generally intense) is that which results in the least dynamic range of the time-dependent analog signal, which is proportional to $I(t)\sigma$. The recording system capability is 5 decades with decreasing accuracy in the lowest (linear) portion. Fluctuation in fission cross sections, for example, can reach 3 decades in the resonance region, so it is clearly desirable to hold the variation of I(t) across this range to less than 2 decades.

If the cross section to be measured were constant (approximately true for scattering cross sections, and for nonthreshold fission cross sections $0.1 < E < 6$ MeV), a constant I(t) would be ideal. On the other hand, if the cross section varies as 1/v (the low-energy flux monitors $^3He(n,p)^3H$, $^6Li(n,t)^4He$, $^{10}B(n,\alpha)^7Li$, or a scattering cross

section where the detector is 1/v), then Eq. (17) shows that a constant E I(E) would serve the purpose.

We conclude that for the recording problem alone, the following current spectrum, expressed in terms of the various representations, would be optimum.

Spectrum Representation	10 eV < E < 0.1 MeV	0.1 < E < 6 MeV
I(t)	1/t	const
I(E)	1/E	$1/E^{3/2}$
E I(E)	const	$1/\sqrt{E}$

Figures 2 and 3 show that the functional variation for E < 0.1 MeV is approximately correct because of the 1/E slowing-down spectrum produced by the moderator. Above 0.1 MeV, the actual fluxes are larger than this optimum.

4. FISSION FLUX MONITORS

The most suitable flux monitor for fission cross-section measurements is one employing a well-known fission reaction. Because considerable effort has been put forth to obtain high precision cross-section values for $^{235}U(n,f)$,[7-9] this reaction is an obvious choice. The use of a reaction similar to that being investigated has clear advantages in reduction of systematic errors.

In any case, backgrounds present at early times make it imperative that signals be large at high energies. The background is measured by allowing the neutron beam to pass through a blank foil backing, using identical geometry and detectors, and the early-time flux monitor signals must be sufficiently larger than the background so that the subtraction does not result in unacceptable uncertainties. Use of the fission reaction, which typically yields ~85 MeV per fragment,[10] is a convenient way to generate high signal levels.

Below a few keV, fluctuations in the $^{235}U(n,f)$ cross section compromise its use as a flux monitor. Nevertheless, the low-energy $^{235}U(n,f)$ signals can be used together with a flux generated from the light-nuclei (n,p) and (n,α) reactions to derive the $^{235}U(n,f)$ cross section, which can be integrated over standard energy intervals and compared to data of other experimenters to furnish a check on the low-energy flux.

The fission-fragment energy observed as current from the silicon detectors is less than the fragment kinetic energy released in fission because of three factors: (1) energy loss in the fissile deposit, (2) energy loss in the detector front dead layer, and (3) incomplete conversion of fragment energy into observable electron-hole pairs in the silicon, termed fragment energy defect. The combined result of these factors has been measured[3] in a thermal neutron beam using the same ^{235}U oxide foil as one of the underground experiments, and five of the same detectors, with window thicknesses from 0.9 to 3.1 μm. Using the empirical relation of Viola and Seaborg[10] for the initial kinetic energy, and using a nominal value of 12.4 MeV for average energy loss emerging at 45° through half the thickness of a 1 mg/cm^2-dense foil, gives (in MeV)

$$E_{dep} = \left(0.1064\,\frac{Z^2}{A^{1/3}} + 23.2\right)/2 - 12.4\left(\rho_s - 0.586\ \mathrm{mg/cm^2}\right) - 17.1 - 8.3\,d,$$

$$= 0.0532\,\frac{Z^2}{A^{1/3}} + 1.8 - 12.4\,\rho_s - 8.3\,d, \qquad (18)$$

where A is the compound nucleus mass, ρ_s the surface density of the target (oxide) in mg/cm^2, and d the detector window thickness in μm. Uncertainties in this expression result from standard deviations of these measurements of E_{dep}, ρ_s, and d, and the errors of extrapolation away from ^{235}U and away from $\rho_s = 0.586$ mg/cm^2. Taking a 10% uncertainty in the coefficient of $Z^2/A^{1/3}$, 30% in the estimate of dE/dx, ± 0.1 μm in d, and ± 0.6 MeV in E_{dep} from the thermal measurements, we get

$$(\delta E_{dep})^2 = \left[0.005\left(\frac{Z^2}{A^{1/3}} - 1370\right)\right]^2 + (12.4\,\delta\rho_s)^2 + \left[3.7(\rho_s - 0.586)\right]^2 + (0.83)^2 + (0.6)^2\,(1.92 + 0.81\,d + 0.38\,d^2). \qquad (19)$$

Thus, the observed average kinetic energy per fragment from the standard ^{235}U foil in a 1-μm window detector is 59.0 ± 1.3 MeV. For neutron bombarding energies of interest, the kinetic energy of fission fragments is independent of excitation energy, so the quantity $E_{dep}(E)$ in Eq. (8) is a constant; recall, however, that there are two fragments of energy E_{dep} per fission event.

5. MONITORS FOR LOW-ENERGY NEUTRONS

Below 1 to 10 keV, light nuclei are more suitable for flux monitors because their cross sections

are smoother than fission cross sections. Relatively low signal levels are acceptable because backgrounds are negligible. Desirable attributes of the flux monitor include a large, smooth, well-known reaction cross section, a high reaction energy, and small energy loss for the detected particles. The last quantity depends on the physical and chemical form of the foil. Three familiar candidates immediately present themselves: $^{3}He(n,p)^{3}H$, $^{6}Li(n.t)^{4}He$, and $^{10}B(n,\alpha)^{7}Li$. Advantages and disadvantages of each are discussed below.

As each of these reactions involves the detection of a relatively low-energy charged particle, careful attention must be paid to the energy losses of charged particles in matter. The stopping cross section, ϵ, in eV-cm^2/molecule can be expressed[11] as

$$\epsilon(E_c) = -\frac{1}{N}\frac{dE_c}{dx} = a(\ell n\, E_c + b)/E_c \qquad (20)$$

where for protons and for atomic number Z the constant a is 0.2395 Z x 10^{-15} MeV-eV-cm^2/atom, and b is about 5 - ln Z if E, the particle energy, is in MeV. For molecular foils or for very low particle energies, this expression has no physical meaning, but values of a and b can be found to fit experimental data[11] over the ranges of interest.

The foils used are thick enough that ϵ varies considerably over the thickness $N_s = Nx$. Expanding the particle energy in powers of N_s,

$$E_c(N_s) = E_{c0} + N_s\left(\frac{dE_c}{dN_s}\right)_{E_{c0}} + \frac{1}{2}N_s^2\left(\frac{d^2E_c}{dN_s^2}\right)_{E_{c0}} + \cdots .$$

But $dE_c/dN_s = -\epsilon$

$$\frac{d^2E_c}{dN_s^2} = -\frac{d\epsilon}{dN_s} = -\frac{d\epsilon}{dE_c}\frac{dE_c}{dN_s} = \epsilon\frac{d\epsilon}{dE_c} \qquad (21)$$

Differentiating Eq. (20), the average energy loss in half the thickness (atoms/cm^2) is

$$\Delta E_c = \epsilon(E_{c0})\frac{N_s}{2} + \frac{1}{2}\frac{\epsilon(E_{c0})}{E_{c0}}\left[\epsilon(E_{c0}) - \frac{a}{E_{c0}}\right]\left(\frac{N_s}{2}\right)^2 + \cdots \qquad (22)$$

This approximation has been compared to a calculation by D. W. Watkins of this Laboratory, in which the foil was divided into a large number of zones and the average emerging energy was found by considering the particles that originated in each zone and passed sequentially through other zones to the surface. The approximation was adequate for the foil thicknesses used. An error of 10% of the calculated ΔE_c is assigned to the result; because ΔE_c varies with the incident neutron energy, it is included with the statistical, rather than the systematic, errors. Relevant values of a and b are discussed below and listed in Table II.

The quantity $E_{dep}(E)$ for Eq. (8) is found by solving the nuclear kinematics for the initial energy, E_3, of the detected particle of mass M_3:

$$E_3(E) = \left\{\frac{(M_3E)^{1/2}}{A+1}\cos\theta_L + \left[\frac{A+1-M_3}{A+1}Q + \frac{A-M_3}{A+1}E + \frac{M_3E}{(A+1)^2}\cos^2\theta_L\right]^{1/2}\right\}^2 . \qquad (23)$$

Equations (20) and (22) are evaluated at E_3, and

$$E_{dep}(E) = E_3(E) - \Delta E_c(E_3). \qquad (24)$$

a. The $^{3}He(n,p)^{3}H$ Reaction

The large thermal cross section, 5327 ± 10 barns, is known to vary as 1/v up to 11 eV,[12] and although there are no published measurements of energies between this and 5 keV, a good theoretical extrapolation of the data[13] gives confidence to within a few per cent. The Q-value is 0.764 MeV. The stopping-power parameters a and b given in Table II are from Ref. 11.

A ^{3}He gas target was used as a flux monitor in the Persimmon event. The atomic density was found by measurement of temperature and pressure, and the chamber was arranged with the detectors within the gas[14] at 90° to the beam; tritons do not contribute to the signal for E $\lesssim$ Q. The energy loss in the gas for this experiment is shown in Table II; note that the thickness Δx is the total gas between the center of the active area and the detector. The active areal density was 9.13 x 10^{18} atoms/cm^2. The additional energy loss in a 1-μm silicon detector window is also shown in Table II. Because the proton velocity is too low for use of the true Bethe-Bloch expression in silicon, the parameters were fitted by least squares to data in the energy range of interest.

There was a background for E > 2 keV in the Persimmon event which did not appear in the accompanying ^{4}He monitor. As this was probably due to the gamma flash at t = 0, positioning of the source out of the line of sight may help. The geometry used included a ring of detectors around the beam; to first order this corrects for any beam asymmetry. The resulting geometry, however, thus differs from

TABLE II

QUANTITIES USED IN CALCULATION OF E_{dep}

Material	Q (MeV)	Initial E_c for E = 0 (MeV)	a (10^{-15} MeV-eV-cm^2)	b (-ℓn MeV)	Typical Values $N_s/2$ (10^{18} cm^{-2})	ΔE_c (MeV)	E_{dep} (MeV)
^{3}He	0.764	E_p = 0.573	0.479	3.99	26.5	0.080	0.427
^{6}Li	4.786	E_t = 2.735 E_α = 2.051	10.8	1.276	25.0	0.249	1.977 x 2
^{6}LiF	4.786	E_t = 2.735 E_α = 2.051	36.4	1.187	8.0	0.251	1.975 x 2
^{10}B	2.344	$\bar{E}_\alpha$ = 1.492	24.9	1.391	6.0	0.184	1.010
Si	--	E_p > 0.200	2.83	2.850	5.2	0.066	--
		E_α = 0.6 E_t	44.8	0.751	5.2	0.167	--
		$E_\alpha \approx 1.4$	53.5	1.094	5.2	0.298	--

that of most other targets, making comparison slightly more uncertain.

b. ^{6}Li(n,t)^{4}He and ^{6}Li(n,α)^{3}H

Either the triton or the α may be detected from a reaction. The thermal cross section is 940.3 ± 1.6 barns,[15] and σ ∝ 1/v (with increasing uncertainties) to a few keV.[16] The Q-value is 4.786 MeV. Table II includes stopping-power parameters for both lithium metal and LiF; the latter, as a vacuum evaporated foil, has been our principal low-energy flux monitor. Note that if it were feasible to use ^{6}Li metal, three times as much lithium could be used with the same energy loss.

Detection of both the triton and the alpha complicates the energy loss calculations. First, energies of the reaction products emitted at 15, 55, and 90° were calculated for bombarding energies from 0 to 10 MeV. It was found that the average of the α and the t was given to within 0.3% by a single kinematic calculation assuming an emitted particle of mass 3-1/2. To find the stopping power for this imaginary particle, the average of $\epsilon_\alpha(E_\alpha)$ and $\epsilon_t(E_t)$ was plotted vs $E_{av} = (E_\alpha + E_t)/2$ for all of the above bombarding conditions. The plot was extended to slightly lower values of $\bar{E}$ assuming that $E_\alpha = 0.75\ E_t$ (as for zero bombarding energy), and then the parameters a and b were fitted by least squares to the averaged data. The resulting energy-loss calculations agree to within 1% with the average of separate calculations for α and t.

The same procedure was carried out for the silicon detector window, using $E_\alpha = 0.6\ E_t$ (as is the case when the particles leave a typical LiF foil), and considering the energy range of E_{av} from 1.3 to 2.4 MeV, for which ϵ_α and ϵ_t could be derived from data in Ref. 11. The resulting stopping powers are nearly identical to those of LiF, and we have customarily added the silicon atoms to the LiF and made a single calculation. These calculations were checked by bombarding a LiF foil with reactor neutrons and measuring pulse heights in silicon detectors. The calculated average energy loss was within the experimental uncertainties.

The thicknesses given in Table II are half those of typical targets and represent the average amount of material traversed by escaping particles. Note that for ^{6}Li the typical E_{dep} values are for either of the two particles, and should be doubled to give the total detectable energy per reaction.

c. ^{10}B(n,α_0)^{7}Li and ^{10}B(n,α_1)^{7}Li*

The reaction proceeds principally to the first excited state, the ground-state branch being only 6.3% for thermal neutrons[17] and remaining constant up to 30 keV.[18] The average Q-value has been taken to be 0.063(2.792) + 0.937(2.314) = 2.344 MeV. If necessary, the effect of the variation of branching ratio above 30 keV, which produces a slight increase in $\bar{Q}$, can be simulated to first order by a variation in the assumed cross section, because the signal strength depends on the product of σ and E_{dep}. The 2200-m/sec cross section ($\alpha_0 + \alpha_1$) is 3835 ± 7 barns,[19] and the variation is within about 4% of 1/v up to and above 100 keV.[18,20] Stopping-power parameters were fitted to data on proton energy losses[21] adjusted for the α-particle mass and charge.[11] The thickness used in the example is half that of a

200-μg/cm^2 foil. Parameters have also been fitted to silicon data in the appropriate energy range.

This monitor has the advantage that the foil is vacuum-deposited ^{10}B metal.[22] It is therefore physically and chemically stable, and there is no danger of leakage, as in the case of ^{3}He, or flaking, as with ^{6}LiF. It should be possible, with care, to use a foil for years.

d. Comparison of ^{3}He, ^{6}Li, and ^{10}B

The three flux monitors should be compared on the basis of the criteria discussed earlier--the relative detected event rate per resolved time interval (statistics), and the energy deposition rate (signal level). Because each event produces only a very small signal, satisfaction of the latter criterion ensures satisfaction of the former. For a given neutron energy, E, the signal level is proportional to

$$\sigma_s \, \sigma(E) \sqrt{E} \, E_{dep}(\rho_s, E, Q).$$

The quantity $\sigma(E)\sqrt{E}$ is a constant for each reaction over the 1/v range of its cross section. Note that E_{dep} is a function of foil density ρ_s as well as of E and Q. A curious fact is that for these three reactions, the product $\sigma_0 E_{dep}$ is nearly the same; for the values of N_s used in Table II, it differs by 5% between ^{6}Li and ^{10}B, and slightly more between these and ^{3}He. This holds until the foil thickness approaches the range of the primary energy-carrying particle as is shown in Fig. 4.

One might conclude from Fig. 4 that ^{6}LiF or ^{6}Li metal foils hold a distinct advantage. This would be true except that foils of ^{6}LiF cannot easily be made appreciably thicker than 0.01 x 10^{21} molecules/cm^2, and that ^{6}Li metal foils present many practical difficulties. ^{6}LiF foils of essentially infinite thickness can be made if some internal structural support is provided. The response is more complex than that of a thin, pure target, but such foils may be used to advantage in transmission measurements (see Section 8).

At present, we feel that the reactions ^{3}He(n,p)^{3}H, ^{6}Li(n,t)^{4}He, and ^{10}B(n,α)^{7}Li have roughly equal merits for use as flux monitors at low neutron energies. This may no longer be true if the background generated by the gamma flash can be reduced,[14] or if the monitors are used at higher neutron energies where the angular distributions of the emitted particles become an important factor.

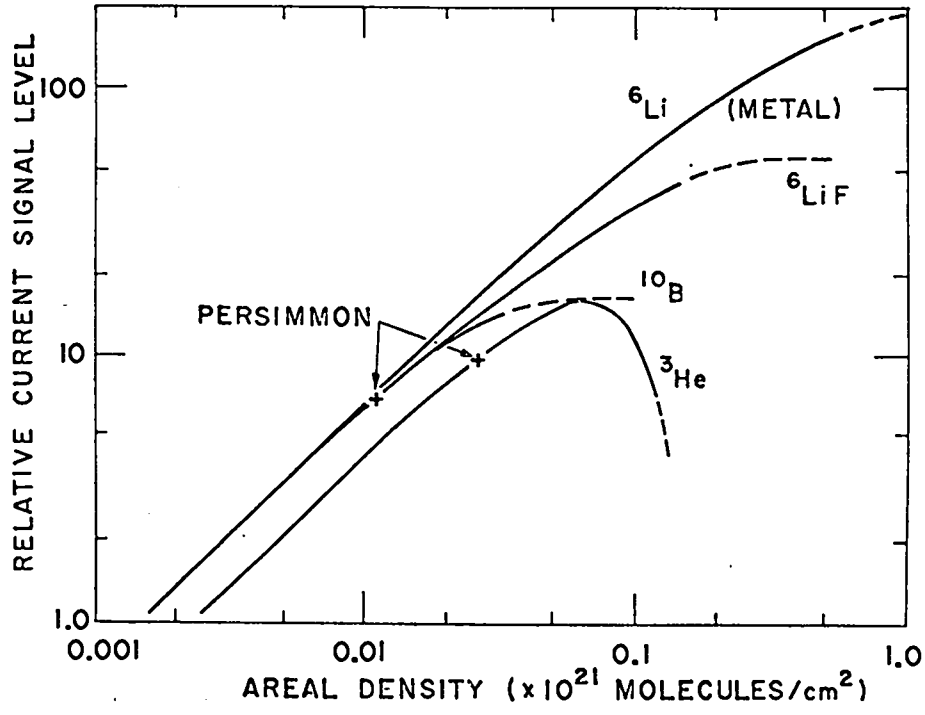

Fig. 4. Comparison of alternative materials for flux measurement at low neutron energies, in terms of relative signal level vs areal density of the target material.

6. SCATTERING FLUX MONITORS

Although the flux determined by fission and light-element (n,p) and (n,α) reactions might be used for scattering reactions, the use of a known scattering reaction for the flux monitor has the advantage of canceling uncertainties in $E_{dep}(E)$ and background by the use of identical detectors for the monitor and the unknown signal. The quantity $E_{dep}(E)$, average detected energy per scattered neutron, is a complicated function of energy including cross section and kinematics of the reaction used to convert the scattered neutron to a detectable charged particle and the energy loss of that particle before detection. Clearly, a thicker target must be used, and the scattered-neutron detector must have a relatively high efficiency because of the low signal levels obtainable per detected event. In principle, the same reactions used for direct flux measurement can also be used to detect scattered neutrons, and the discussions of Sections 4 and 5 are applicable.

a. Scattered-Neutron Detectors

A high-pressure ^{3}He gas scintillation detector[23] has been successfully used for measurement of scattering cross sections. Operating at 240 atm, the detector has high neutron efficiency and low sensitivity to gamma radiation. Another form of detector using ^{3}He, which will be used in the next experiment, has a stack of 10 silicon detectors in a vessel filled with ^{3}He at about 25 atm, at which pressure the range of the emitted proton is equal to the distance between detectors. The characteristics of this type of detector arrangement have been studied elsewhere,[24,25] and look promising for this application.

Another possibility involves placing ^{235}U foils between the silicon detectors in the stack. Since the ^{235}U cross section is far from smooth, a block of polyethylene (1 cm thick) would be placed in front of the detector to spread the energies of the incident neutrons. Unfortunately, the polyethylene also prevents a large fraction of the neutrons from reaching the detector, so that the signal level would be no larger than the ^{3}He signal.

The above detectors are sensitive to fission neutrons as well as scattered neutrons. To measure scattering from a fissile target, a second detector stack with CH_4 gas could be used to measure the fission neutrons for subtraction from the signal from a similar stack in ^{3}He. This subtraction will also correct for γ-ray background. Because the two signals will be nearly equal, it would be advantageous to balance the detector responses very carefully and subtract the analog signals before recording.

b. Monitor Target

The ^{209}Bi(n,n) reaction offers several advantages as a flux monitor for scattering cross-section measurements. Natural bismuth is monoisotopic and has a constant, relatively large, well-known cross section. The capture cross section is small. A large scattering resonance at 800 keV will verify the energy scale and the resolution of the system. The thickness of the Bi can be determined by weighing. Lead is a possible alternative to bismuth, although its capture cross section is slightly larger.

7. CAPTURE FLUX MONITOR

On all experiments to date, the flux determined by fission and light-nuclei monitors has been used for the capture cross-section measurements as well. This has not been adequate because systematic errors are introduced by the use of gamma detectors with characteristics differing from the flux detectors. The situation is expected to be improved on the next shot by using identical detectors to measure flux at several points in the spectrum by observing known resonances in a monitor target.

The ideal detector for capture measurements in these experiments would have a high efficiency independent of the incident photon energy; its response would thus be independent of the cascade following capture in any particular isotope. The detector used is of the Moxon-Rae type,[26] with Bi_2O_3 added to the graphite converter to flatten the energy response,[27] and with a solid-state detector,[28] replacing the photomultiplier of the original design. This design is expected to have a constant response per MeV of incident gamma energy for photons between 1 and 8 MeV.

Calculation of the efficiency of this detector to better than about ±20% is difficult.[3] An efficiency measurement will be attempted in our next experiment:[29] the neutron beam will be passed through gold and ^{238}U foils mounted inside a rapidly rotating drum. The tangential velocity of the foil will be sufficient to resolve capture resonances between 40 and 330 eV, so that each of the activated

resonance areas may be cut out (in the manner of the Los Alamos "wheel" experiments),[30] and the activity of each determined by standard counting methods. From the residual ^{198}Au and ^{239}Np β-activities, the total number of captures that occurred in each resonance will be determined. Multiplying the number of captures in each resonance by the gamma energy and by the calculated geometric solid angle of the converter gives the total energy that struck the converter. Signals from Moxon-Rae detectors viewing the reaction area on the foil will be recorded in the normal fashion, giving the total converted electron energy deposited in the detectors. The efficiency, e, is simply the ratio of the observed electron energy to the calculated γ-energy, and the quantity $E_{dep}(E)$ to be used in Eq. (8) is

$$E_{dep}(E) = \left(Q + \frac{A}{A+1} E\right)e. \qquad (25)$$

This efficiency measurement will permit use of a (stationary) gold foil as a capture flux monitor as long as the design of the Moxon-Rae detectors is not altered.

8. TOTAL CROSS SECTION BY FLUX MEASUREMENT

Total cross sections can be measured by comparing flux measurements made simultaneously on both sides of a sample in the neutron beam. Suppose that $I_1(t)$ and $I_2(t)$ are signals from two essentially identical flux monitors and that α is the relative normalization factor of the two monitor detectors. Then

$$\alpha\, I_2(t) = I_1(t)\, e^{-N_s \sigma_T(E)}, \qquad (26)$$

and we may write for the transmission ratio, T,

$$T = \exp(-N_s\sigma_T) = \frac{\alpha\, I_2}{I_1} = \alpha\left(1 - \frac{I_1 - I_2}{I_1}\right), \qquad (27)$$

$$\sigma_T(E) = \frac{1}{N_s} \ln \frac{1}{T}. \qquad (28)$$

To determine the precision with which such a cross section can be measured, consider first the case in which the signals $I_1(t)$ and $I_2(t)$ are recorded separately. The nominal uncertainty of any signal recorded within the logarithmic region of the amplifier characteristic, including comparison to the calibration signal, is ±4%, and we may assume that α can be measured to ±2%. If the two foils are similar thicknesses of the same material, uncertainties in monitor cross section and $E_{dep}(E)$ cancel; if, further, the uncertainties in background subtraction are negligible, the result is

$$\delta T/T = \left[(4\%)^2 + (4\%)^2 + (2\%)^2\right]^{1/2} = \pm 6\%$$

for any value of T large enough to keep $I_2(t)$ within the log region. By differentiating Eq. (28),

$$\frac{\delta\sigma}{\sigma} = \left|\frac{1}{\ln T}\right|\frac{\delta T}{T} = \frac{1}{N_s\sigma_T}\frac{\delta T}{T}, \qquad (29)$$

so that for high transmission the resulting uncertainty in σ_T is great. To keep the recording uncertainty below 10%, the transmission must be less than 55%, or $N_s\sigma_T$ must be greater than 0.60.

The final equality in Eq. (27) indicates the possibility of recording the difference signal, $I_1 - I_2$, rather than I_2 itself. Several new difficulties arise. (1) The time difference between the two signals becomes significant at moderate to low energies, being 4 μsec for 50-eV neutrons if the two detectors are separated by 0.4 m. (2) Because $I_1 \approx I_2$, the difference signal is not usually in the log region of the amplifier unless α is appreciably greater than 1. (3) The recorded signal, although small, will have statistical fluctuations corresponding to the sum of I_1 and I_2; this may cause broadening of the line recorded on the film. If we limit discussion to energies above 100 eV, take $\alpha \gtrsim 1.03$, and assume smoothing of ~ 2 μsec on the amplifier inputs, we can calculate the best obtainable recording precision by propagation of errors in Eq. (27).

$$\delta T/T = \left\{(2\%)^2 + \left(\frac{1}{T} - 1\right)^2\left[(4\%)^2 + (4\%)^2\right]\right\}^{1/2},$$

where $\delta\alpha/\alpha$ has been taken to be ±2% and each recording is assumed good to ±4%. Applying Eq. (29), we find the range of transmission values over which $\delta\sigma/\sigma \lesssim 10\%$ to be $0.35 < T < 0.75$, corresponding to $0.3 \lesssim N_s\sigma_T \lesssim 1.0$.

It appears that some advantage may be gained by use of ^6LiF foils that are effectively infinitely thick. The tendency of LiF targets of this thickness to crack and flake necessitates some type of internal structural support. Larry D. Allen of this Laboratory has achieved some success in making targets in the 6- to 7-mg/cm^2 LiF range by using backing foils etched in a crosshatch pattern to provide the needed support.

These foils yield signal currents about five times as high as the thin (0.4-mg/cm^2 LiF) foils

normally employed. If the foils are thicker than the range of the particles, the signal does not depend on the thickness. However, estimation of the average energy loss per micrometer of the silicon detector window is very complicated because particles of all energies from zero to maximum are present. Therefore it is probably not feasible to make an absolute flux determination from a thick foil. A difference signal, on the other hand, can be measured if the two detectors are carefully selected to have identical windows.

9. DATA REDUCTION

The computer programs for data reduction are described generally in Ref. 3. Once the data recordings have been digitized and converted to the signal (mV) vs time (μsec) form, the SIGER (SIGma and ERror) program may be used to find the flux by any of the methods given in Sections 4 through 8. The basic functions of SIGER are to convert the time to energy by Eq. (1), to average signal readings within time channels of a specified width, to subtract a background and divide by a reference (e.g., cross section) interpolated at the appropriate energy, to normalize, and to estimate statistical errors and propagate them through all operations. The experimenter selects program options by the values of constants and the background and reference functions that he supplies.

Combining Eqs. (6) and (8) and solving for I(t),

$$I(t) = \frac{V(t)/\left(\Omega_L N_s R_{amp} \times 4.43 \times 10^{-8}\ \mu C\text{-MeV}^{-1}\right)}{E_{dep}(E)\ \omega(\theta_L,\theta_C)\ \frac{d\sigma}{d\Omega_C}(E,\theta_C)}. \quad (30)$$

Expressing the background subtraction explicitly and using in part the notation of SIGER,

$$I(t) = \frac{V(t)/EFF - BKG(E)/EFBKG}{E_{dep}(E)*OMEGA*REF(E)/EFREF}, \quad (31)$$

where OMEGA = $\omega(\theta_L,\theta_C)$; the relative efficiencies EFF, EFBKG, and EFREF, as given, include the numerical and geometric factors in Eq. (30); and BKG(E) and REF(E) are tabulated functions with corresponding relative errors also tabulated. Functions BKG and REF are usually either constants, known cross sections, or signals previously processed by SIGER. Note that the output, I(t), is tabulated vs E rather than t. The calculated standard deviation in I(t) is

$$\frac{\delta I}{I} = \left[\frac{(\delta V/EFF)^2 + (\delta\ BKG/EFBKG)^2}{(V/EFF - BKG/EFBKG)^2} + \left(\frac{\delta E_{dep}}{E_{dep}}\right)^2 + \left(\frac{\delta\ REF}{REF}\right)^2 + (CORR)^2\right]^{1/2}, \quad (32)$$

where δV is the quadratic sum of the calibration error (uncertainty in readings of the data and calibrations, provided as input to the program) and the statistical error calculated as the larger of the statistics on the counting rate and the rms deviation of the readings within the time channel, and CORR is the correlated or systematic error, including standard deviations of Ω_L, N_s, and R_{amp}.

Taking arbitrary standard values of 0.2816 sr for Ω_L and 51.1 ohms for R_{amp}, the usual definition used for EFREF is

$$EFREF = \frac{4\pi/(N_s \times \text{fragments per event})}{0.2816 \times 51.1\ \frac{V\text{-}\mu sec}{\mu C} \times 4.43\times10^{-8}\ \mu C/MeV} = \frac{19710/\text{fragments}}{N_s(\times10^{15}\ \text{atoms/cm}^2)}\ \frac{MeV\text{-}b}{mV\text{-}fsec}. \quad (33)$$

The relative signal efficiency, EFF, is then

$$EFF = \frac{\Omega_L}{0.2815}\ \frac{R_{amp}}{51.1}\ \frac{\ell_{ref}}{\ell}, \quad (34)$$

where the distance ℓ_{ref} is the flight path to an arbitrary reference target position, and the ratio ℓ_{ref}/ℓ is included to correct for the difference in the time-energy conversion between this position and the signal, V(t), position. The BKG signal is generally already normalized to the standard detector solid angle by Eq. (34); any further normalization required is included in EFBKG. When the V(t) of a background signal is run to obtain the BKG function, BKG is set to zero and REF to unity; CØRR should include the uncertainty in the values of EFBKG to be used in subsequent signal analyses.

The several types of flux measurements will now be discussed individually.

a. Fission

The average energy per fragment, E_{dep} (called EBAR in SIGER), may be entered directly, in which case its uncertainty is included in CORR, or is calculated from Eq. (18) if Z, A, ρ_s, and d are given. In the latter case, the uncertainty is calculated from Eq. (19) assuming that $\delta\rho_s/\rho_s$ = 10%; if the uncertainty in ρ_s is significantly different from this, the difference can be included in CORR. Note that ρ_s (mg/cm^2) is the total density of the foil

deposit, normal to its backing, while the N_s used in Eq. (33) is the number density ($\times 10^{15}$ atoms/cm^2) of nuclei of the target isotope along the beam direction, so that N_s must include a factor $\sqrt{2}$ if the target is inclined 45° to the beam.

The REF function is a tabulation of measured cross section, $\sigma_f(E)$, or, if the angular distribution is important, is $4\pi \frac{d\sigma}{d\Omega_c}(\theta_c)$.

b. Low Energy

The use of SIGER is identical to the fission case except that the program parameter THICK (or THICK2) must be specified so that $E_{dep}(E)$ will be calculated by Eqs. (20) to (24). Values of Q, A, θ_L, a, b, and $N_s/2$ must be supplied (see Table II). If the mass of the detected particle is not (A+1)/2, or if stopping-power parameters a, b, and N_s are required for a second material (i.e., the silicon detector window), then THICK2 is specified and the required values are read from another card. (The second card is needed for all materials except LiF.) Note that $N_s/2$ includes a factor $\sqrt{2}$ for the 45° inclination of the target to the direction of the detected particles. The N_s used here is the value used in Eq. (33) divided by the isotopic purity of the sample to give the total molecular density.

c. Scattering

As stated in Section 6, determination of flux by scattering is complicated by the energy dependence of the detector efficiency, but it is not necessary to know the actual flux to make a cross-section measurement. Setting EBAR = 1 and REF(E) = monitor cross section causes analysis of the monitor signal by SIGER to produce the function to be used as REF(E) in reducing the unknown signals, which would also be run with EBAR = 1.

It is also possible to remove the energy dependence of the detector cross section and detected particle energy approximately. Specify THICK so that kinematics will be calculated; with Q = 0, elastic scattering will be assumed. If a value of STHERM, the 2200-m/sec cross section of the detector (e.g., ^{3}He), is given, the signal is divided by the 1/v cross section at the energy of the scattered neutron. The charged-particle energy is approximated from Eq. (23) with $M_3 = 1$, $\theta_L \approx 15°$, and $A \approx 3$:

$$E_{dep}(E_3) = \tfrac{3}{4}Q + 0.617E_3 + \sqrt{\tfrac{3}{15}E_3(Q+0.744E_3)} - \Delta E_1 - \Delta E_2, \quad (35)$$

where Q of the detecting reaction is given to the program as EBAR, E_3 is the scattered-neutron energy, and energy losses in one or two materials may be calculated as in b above. Because errors cancel when ratios are taken, no uncertainty is calculated for Eq. (35). EFREF must include the density, N_d, of detector nuclei and the solid angle ratio, $2\pi/4\pi$, for detecting particles:

$$EFREF = \frac{39420}{N_s(\times 10^{15}\ \text{atoms/cm}^2)N_d(\text{atoms/b})} \frac{\text{MeV-b}^2}{\text{mV-fsec}}. \quad (36)$$

The resulting signal is a neutron current, more or less directly comparable to determinations by other methods. It may be used as REF(E) in reduction of unknown signals if THICK, Q = 0, STHERM, EBAR = $Q_{detector}$, and EFREF are similarly specified.

d. Capture

To calculate kinematics by Eq. (25), the emitted particle mass M_3 must be set to zero. This can be done only by specifying THICK2 and punching an explicit 0 on the card. Q and A are given as usual, and EFF is calculated by Eq. (34). The conversion efficiency, e, is included in EFREF.

$$EFREF = \frac{19710/e}{N_s(\times 10^{15}\ \text{atoms/cm}^2)}$$

$$\approx \frac{0.02}{N_s(\text{atoms/b})} \frac{\text{MeV-b}}{\text{mV-fsec}}, \quad (37)$$

where the value $e \approx 0.001$ is a result from Petrel,[3] and will be determined with greater accuracy on future experiments. Uncertainty in e cancels when ratios between identical detectors are taken. BKG and REF have their usual meaning.

e. Total

If a value of reciprocal sample thickness (BPA) in barns per atom is given, SIGER assumes that V(t) and REF(E) in Eq. (31) are signals from targets of the same material following and preceding the sample, respectively, and determines the cross section from Eq. (28). All other input program data are the same as those for determining flux in the manner appropriate to the target. The function REF(E) must have been previously processed by SIGER without being divided by the cross section; i.e., the REF used was unity and the result was I · σ, rather than I.

If the targets before and after the sample are

not the same substance, or if only the actual current is available to use for REF(E), a special-purpose REF(E) that is the product $I \cdot \sigma$ can be constructed by an auxiliary program. Alternatively, if the cross section of the material following the sample varies as 1/v, its value at 2200 m/sec, STHERM, may be entered as data, in which case the signal is divided by σ as well as by REF(E), and REF(E) may be the neutron current.

If the difference (before - after) and one of the signals are recorded, Eq. (27) can be cast into the form of Eq. (31) as follows.

$$T = \frac{\alpha I_2}{I_1} = \frac{(I_1-I_2) - I_1}{I_1/(-\alpha)} = \frac{I_2}{[(I_1-I_2) + I_2]/\alpha}.$$

The functions BKG and REF are chosen to reconstruct the transmission ratio. The errors in this recording mode are discussed in Section 8.

10. AVERAGE OF FLUX DETERMINATIONS

In general, two or more detectors view each monitor target, two recordings of each signal are made, and two or more readings (digitizations) are made of each recording. Thus it may be desirable to average together eight or more flux functions from a single target; and, further, it may be necessary to combine determinations from various targets to find "the flux" for a given experiment. The GRAV (GRaphing and AVeraging) program performs the averaging with due consideration for the standard deviation carried by each point.

To minimize the standard deviation of the result, each point in the average must be weighted inversely as the square of its uncorrelated (random) error. GRAV subtracts the square of the correlated error from the square of the total error, performs the required arithmetic and propagation of errors, and then recombines the correlated error (which is not necessarily the same as the input value) with the result. The correlated error is the quadratic sum of all sources of uncertainty that affect every data point equally. Note that the correlated part of the error calculated in SIGER by Eq. (32) is greater than the value of CORR given as program input; it also includes the correlated parts of $\delta REF/REF$, $\delta E_{dep}/E_{dep}$, and the calibration error. This larger value must be used as input to GRAV.

The correlated error of GRAV output depends on the degree to which the inputs are correlated among themselves. The general prescription is to combine each contribution to correlated error which is identical for all readings, with the rms of the values for each of the contributing factors which is independent among readings. Thus, if several readings or recordings of the same signal are being averaged, only the calibration error is independent; the output CORR is the quadratic sum of the rms of the correlated parts of the calibration errors and the common value of the input correlated error of each reading omitting the calibration error. For two detectors viewing the same target, two such GRAV outputs would then be averaged together, and the final CORR might be written as

$$CORR^2 = \left(\frac{\delta N_s}{N_s}\right)^2 + \frac{1}{2}\left[\left(\frac{\delta R_{amp}}{R_{amp}}\right)_1^2 + \left(\frac{\delta R_{amp}}{R_{amp}}\right)_2^2\right] + \frac{1}{2}\left[\left(\frac{\delta \Omega_1}{\Omega_1}\right)^2 + \left(\frac{\delta \Omega_2}{\Omega_2}\right)^2\right] + \left(\frac{\delta\ REF}{REF}\right)^2 + \left(\frac{\delta\ E_{dep}}{E_{dep}}\right)^2 + \frac{1}{2}\left[\left(\frac{\delta\ CAL}{CAL}\right)_1^2 + \left(\frac{\delta\ CAL}{CAL}\right)_2^2\right],$$

where only the correlated parts of δ REF and δE_{dep} are included, and the δ CAL/CAL's are the rms values for the respective signals.

In addition to calculating an "internal" uncorrelated error by propagation of errors, GRAV also calculates an "external" error as the rms deviation of the points from their average. The larger of these two uncertainties is combined with the output correlated error to obtain the output standard deviation of each point. The internal and external errors should be roughly equal; if not, they indicate improper error assignment or handling.

The final task is to choose from the various flux determinations to obtain "The Flux." This is largely a matter of judgment, and the procedure varies from experiment to experiment. As an example, consider the Persimmon flux:

10^6 to 10^4 eV, used three (of four) high-resolution readings of two detectors on ^{235}U, CØRR = 4.2%;

10^4 to 1000 eV, used six (of eight) ^{235}U readings, CØRR = 1.8%;

1000 to 100 eV, used 12 readings from three dedetectors on ^{6}Li, CØRR = 4.2%;

100 to 13 eV, read points of a graph of ^{3}He result, normalized to give correct integrals for ^{235}U cross section

as determined from two signals,

CØRR = 1.2%.

The flux deck so compiled is suitable for use in determining unknown fission and charged-particle cross sections, and (with doubtful normalization) for capture measurements. For scattering and total measurements, special fluxes must be derived as discussed in Section 9.

ACKNOWLEDGMENTS

We are grateful for the close cooperation of Delmar W. Bergen and the unflagging support of Mrs. Nancy Browne in this work. Basic to any large-scale effort, particularly these nuclear explosion time-of-flight measurements, are the continuing contributions of many colleagues in every phase of the work from mechanical design to data analysis. These colleagues, for the most part members of Groups P-3 and W-8 led by Benjamin C. Diven and Arthur Hemmendinger, are responsible for the success of these experiments. We are particularly grateful to many individuals in the test division for their support.

REFERENCES

1. A. Hemmendinger, B. C. Diven, W. K. Brown, A. Ellis, A. Furnish, E. R. Shunk, and R. R. Fullwood, "Time-of-Flight Neutron Cross-Section Measurements Made with Neutrons from Nuclear Explosions," LASL report LA-3478, Part I, 1968. For a simplified review of the method and the present status of all measurements, see: W. K. Brown and G. A. Cowan, "Scientific Applications of Nuclear Explosions," from Proc. Symp. Education for the Peaceful Uses of Nuclear Explosives, Tucson, Arizona, March 31 to April 2, 1969, University of Arizona Press.
2. W. K. Brown and A. P. Furnish, "A High-Resolution Recording System for Neutron Cross-Section Measurements Using an Underground Nuclear Explosive Source," IEEE Trans. NS-16, 411 (February 1969).
3. P. A. Seeger and D. W. Bergen, "Time-of-Flight Neutron Cross-Section Measurements Using Nuclear Explosions," LASL report LA-3478, Part II, 1967.
4. H. A. Sandmeier and G. E. Hansen, "Thermal Neutron Spectra from an Underground Nuclear Explosion with Special Consideration of Spectral Modification Due to Bomb Debris Motion," LASL report LA-3403, 1965.
5. R. H. Pehl, F. S. Goulding, D. A. Landis, and M. Lenzlinger, "Accurate Determination of the Ionization Energy in Semiconductor Detectors," Nucl. Instr. Meth. 59, 45 (1968).
6. J. Terrell, "Prompt Neutrons from Fission," Proc. Symp. Phys. Chem. Fission, Vol. II, IAEA, Vienna, 1965.
7. P. H. White, "Measurements of the ^{235}U Neutron Fission Cross Section in the Energy Range 0.04-14 MeV," J. Nucl. Energy, Parts A/B, 19, 325 (1965).
8. G. de Saussure, R. Gwin, L. W. Weston, R. W. Ingle, R. R. Fullwood, and R. W. Hockenbury, "Measurement of the U^{235} Capture-to-Fission Ratio, α, for Incident Neutron Energies from 3.25 eV to 1.8 keV," Nucl. Sci. Eng. 23, 45 (1965). Oak Ridge National Laboratory report ORNL-TM-1804 (1967) by these authors, gives complete numerical results.
9. W. G. Davey, "Selected Fission Cross Sections for ^{232}Th, ^{233}U, ^{234}U, ^{235}U, ^{236}U, ^{237}Np, ^{238}U, ^{239}Pu, ^{240}Pu, ^{241}Pu, and ^{242}Pu," Nucl. Sci. Eng. 32, 35 (1968).
10. V. E. Viola, Jr., and G. T. Seaborg, "Nuclear Systematics of the Heavy Elements," J. Inorg. Nucl. Chem. 28, 697 (1966).
11. W. Whaling, "The Energy Loss of Charged Particles in Matter, Handbuch der Physik, Ed. S. Flügge, (Springer-Verlag, Berlin-Göttingen-Heidelberg, 1958) Vol. XXXIV, p. 193.
12. J. Als-Nielsen and O. Dietrich, "Slow Neutron Cross Sections for He^3, B, and Au," Phys. Rev. 133, B925 (1964).
13. F. L. Shapiro, "Energy Dependence of the Reaction Cross Sections for Slow Neutrons," Soviet Physics JETP 7, 1132 (1958). See also J. Als-Nielsen, "Neutron Cross Sections for He^3 in the Energy Range 0-10 MeV," ENEA Neutron Data Compilation Centre Newsletter CCDN-NW/6 (September 1967).
14. W. K. Brown, A. N. Ellis, and D. D. Peterson, "A 90° ^3He Neutron Spectrometer," IEEE Trans. NS-15, 404 (February 1968).
15. C. A. Uttley and K. M. Diment (Harwell), to be published.
16. A. Bergström, S. Schwarz, L. G. Strömberg, and L. Wallin, "Remarks on the $^6Li(N,\alpha)^3H$ Cross Section in the Region $1 < E_n < 600$ keV," ENEA Neutron Data Compilation Centre Newsletter

CCDN-NW/3 (October 1966).

17. A. J. Deruytter and P. Pelfer, "Precision Determination of the Branching Ratio and Q-Value of the $^{10}B(n,\alpha)^{7}Li$ Reaction and of the Q-Value of the $^{6}Li(n,\alpha)^{3}H$ Reaction," J. Nucl. Energy 21, 833 (1967).

18. K. Gubernator and H. Moret, "Evaluation of the $^{10}B(n,\alpha)$ Cross Section and Branching Ratio," Euratom report EUR 3950 e (1968).

19. A. Prosdocimi and A. J. Deruytter, "A Precise Determination of the Thermal Neutron Absorption Cross Section of B^{10} and Natural Boron by Time-of-Flight," J. Nucl. Energy, Parts A/B, 17, 83 (1963); and G. H. Debus and P. J. Debièvre, "Thermal Neutron Absorption Cross Section of Boron," J. Nucl. Energy 21, 373 (1967).

20. R. L. Macklin and J. H. Gibbons, "Study of $^{10}B(n,\alpha)^{7}Li$, $^{7}Li^{*}$ for $30 < E_n$ keV < 500," Phys. Rev. 165, 1147 (1968). D. Bogart and L. L. Nichols, "Measurement of the $^{10}B(n,\alpha)^{7}Li$, $^{7}Li^{*}$ Relative Cross Sections in the keV Region," NASA technical note NASA TN D-4783 (1968).

21. J. C. Overly and W. Whaling, "Highly Excited States in C^{11} Elastic Scattering of Protons by B^{10}," Phys. Rev. 128, 315 (1962). D. Kamke and P. Kramer, "Energy Loss and Range of Alpha Particles in Boron in the Energy Range from 0.2 to 5.3 MeV," Z. Physik 168, 465 (1962).

22. H. L. Adair and E. H. Kobisk, "Boron Film Preparation Using an Electron Beam Evaporator," from the 1962 Transactions of the Ninth National Vacuum Symposium of the American Vacuum Society, p. 125.

23. R. L. Aamodt, L. J. Brown, and G. M. Smith, "High Pressure ^{3}He Gas Scintillation Neutron Detector," Rev. Sci. Instr. 37, 1338 (1966).

24. M. E. Lee and M. L. Awcock, "A Helium-3-filled Semiconductor Counter for the Measurement of Fast Neutron Spectra," in Neutron Dosimetry Proceedings of the IAEA Symposium at Harwell, England, December 10 to 14, 1962, p. 441.

25. T. R. Jeter and M. C. Kennison, "Recent Improvements in Helium-3 Solid State Neutron Spectrometry," IEEE Trans. NS-14, 422 (February 1967).

26. M. C. Moxon and E. R. Rae, "A Gamma-Ray Detector for Neutron Capture Cross-Section Measurements," Nucl. Instr. Meth. 24, 445 (1963).

27. R. L. Macklin, J. H. Gibbons, and T. Inada, "Neutron Capture Cross Sections Near 30 keV Using a Moxon-Rae Detector," Nucl. Phys. 43, 353 (1963).

28. A. Hemmendinger, M. G. Silbert, and A. Moat, "Transient Response of Solid State Detectors," IEEE Trans. NS-12, 304 (February 1965).

29. A. Ellis, W. K. Brown, J. A. Farrell, and R. R. Fullwood, "Calibration of Moxon-Rae Detectors with Moving Au and U-238 Foils," in progress.

30. G. A. Cowan, A. Turkevich, C. I. Browne, and Los Alamos Radiochemistry Group, "Symmetry of Neutron-Induced U^{235} Fission at Individual Resonances," Phys. Rev. 122, 1286 (1961).